Boolean decision problems with competing interactions on scale-free networks: Critical thermodynamics

Helmut G. Katzgraber,[1,2] Katharina Janzen,[3,4] and Creighton K. Thomas[1,5]

[1]*Department of Physics and Astronomy, Texas A&M University, College Station, Texas 77843-4242, USA*
[2]*Theoretische Physik, ETH Zurich, CH-8093 Zurich, Switzerland*
[3]*Institut für Mathematische Physik, TU Braunschweig, D-38106 Braunschweig, Germany**
[4]*Institut für Physik, Carl-von-Ossietzky-Universität, D-26111 Oldenburg, Germany*
[5]*Department of Materials Science and Engineering, Northwestern University, Evanston, Illinois 60208-3108, USA**

(Dated: September 19, 2018)

We study the critical behavior of Boolean variables on scale-free networks with competing interactions (Ising spin glasses). Our analytical results for the disorder–network-decay-exponent phase diagram are verified using Monte Carlo simulations. When the probability of positive (ferromagnetic) and negative (antiferromagnetic) interactions is the same, the system undergoes a finite-temperature spin-glass transition if the exponent that describes the decay of the interaction degree in the scale-free graph is strictly larger than 3. However, when the exponent is equal to or less than 3, a spin-glass phase is stable for all temperatures. The robustness of both the ferromagnetic and spin-glass phases suggests that Boolean decision problems on scale-free networks are quite stable to local perturbations. Finally, we show that for a given decay exponent spin glasses on scale-free networks seem to obey universality. Furthermore, when the decay exponent of the interaction degree is larger than 4 in the spin-glass sector, the universality class is the same as for the mean-field Sherrington-Kirkpatrick Ising spin glass.

PACS numbers: 75.50.Lk, 75.40.Mg, 05.50.+q, 64.60.-i

I. INTRODUCTION AND MOTIVATION

Networks play an integral role in all fields of science, as well as numerous industrial applications. Virtually any process or group of interacting entities can be described by a network. In particular, the study of *scale-free* networks (i.e., networks where the degree distribution follows a power law) found a renewed interest in the last decades after it had been shown that the internet follows such a network topology [1]. Since then, there have been numerous studies showing that a multitude of networks ranging from computer networks, to protein-protein interaction networks, semantic networks and, in particular social networks such as citation networks or sexual partner networks are also well-described by scale-free networks [2].

Scale-free networks have edge degrees $\{k_i\}$ distributed according to a power law λ, with the probability $\wp_k$ for a node to have k neighbors satisfying

$$\wp_k \propto k^{-\lambda}. \tag{1}$$

A typical network is shown in Fig. 1: While few nodes have many edges connecting them to other nodes, many nodes have few edges; the distribution of these following a power law. Although there have been several studies of Boolean variables on scale-free networks with social interaction networks in mind, most studies have focused on "friend" networks such as, for example, the Facebook [3]

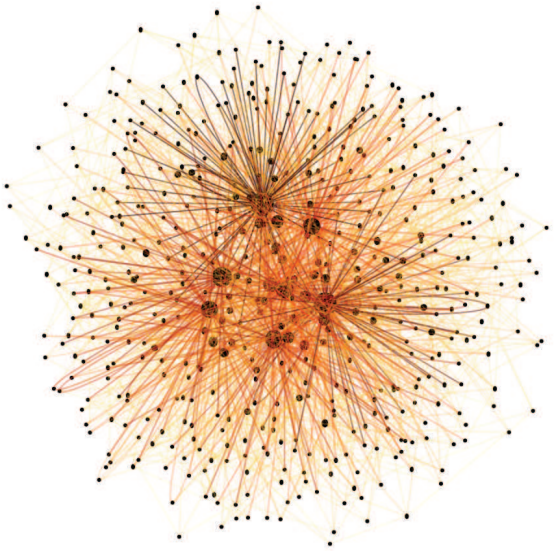

FIG. 1: (Color online) Typical network simulated. The connectivity matrix is selected according to Eq. (1) (i.e., the edge degrees are distributed according to a power law). This explains why few nodes (larger circles) have many connections (darker lines), while many nodes (small dots) have fewer connections (lighter lines). Note that the minimum connectivity in our simulations is 3 (i.e., each node has at least three neighbors and the maximum connectivity scales with the square root of the number of nodes). Data for $N = 512$ nodes.

*present address

network where person A can "friend" person B. Friendship can then be defined via a network edge between A and B with a *positive weight*. However, other networks exist where two persons A and B can either be "friends" or "foes" (i.e., a network with both positive- and negative-weight bonds). This appears, for example, in the slashdot network [4] or when studying the robustness of opinion formation in, for example, an election process. The latter type of network is rarely studied, possibly due to the difficulties introduced by the negative-weighted edges in the system. However, they find wide applicability to many fields of science such as the aforementioned social networks, as well as other applications such as interaction networks between proteins or genes.

Why are Boolean problems on these scale-free networks interesting? Because they can be seen as the simplest model to study how general consensus forms on such a network for a decision problem with two possible outcomes. By placing Boolean variables on each node of the system, one can study either equilibrium or nonequilibrium properties of the thermodynamics of the Boolean variables and thus see how stable a given state of the system is. Generalizations to more complex decision problems can be readily accomplished by replacing the Boolean variables with, for example, q-state Potts variables [5].

The entities interacting on a real network may have complex interactions, but models typically focus on connectivity in randomly occupied networks or on networks with uniform interactions between the entities. As illustrated above and as suggested in different studies [6, 7], many real networks possess both friend and foe interactions among the degrees of freedom. Because the network intrinsically has loops, this leads to frustration between the Boolean variables, quickly complicating the study of such systems.

Here, we study the critical behavior of the random-bond Ising model on scale-free networks. The model maps directly onto a friend or foe network (random bonds) with Boolean variables (Ising spins). Crucially, both ferromagnetic and antiferromagnetic interactions are allowed. Although many of the networks of experimental importance are dynamic and out-of-equilibrium, a thorough understanding of the equilibrium model provides a first step into the understanding of generic problems associated with networks with random interactions.

Monte Carlo simulations of Ising spins on scale-free networks and complex random graphs with *uniform antiferromagnetic* interactions [8–10] have shown that a stable spin-glass phase exists. Similarly, studies of a random-field *ferromagnetic* Ising model [11, 12] on scale-free graphs [13] show that for $\lambda \leq 3$ the spins are always ordered (i.e., consensus is stable to local perturbations), whereas for $\lambda > 3$ a phase transition between a paramagnetic and ferromagnetic phase exists as a function of the random-field strength.

Surprisingly, for the case of a pure Ising spin glass defined on a scale-free graph no detailed numerical results exist with most results relying on analytical approximations and mean-field calculations [14–17]. The detailed mean-field study by Kim *et al.* [15] showed that for $\lambda \leq 3$ the critical temperature of the system diverges (i.e., the spins are stable to arbitrary local perturbations), whereas for $\lambda > 3$ a finite-temperature transition from a paramagnetic to a spin-glass state exists. In this work we *improve* on the results by Kim *et al.* by expanding the approach of Leone *et al.* [18] for ferromagnetic systems to spin glasses. We present analytical results backed up by numerical results (using large-scale Monte Carlo simulations) for both Gaussian-distributed and bimodal edge weights between the Ising spins. We show that when the probability p of positive (ferromagnetic) interactions and the probability $1-p$ for negative (antiferromagnetic) interactions is the same, the system undergoes a finite-temperature spin-glass transition if $\lambda > 3$, in agreement with previous results [15]. However, when $\lambda \leq 3$, a spin-glass (SG) phase is stable for all temperatures. Finally, in the cases where both spin-glass and ferromagnetic (FM) order would be expected ($p > 0.5$), only spin-glass order is present. Relating back to the social Gedankenexperiment, this would suggest that for certain networks the opinion of the individual is robust towards local perturbations and cannot be affected by global consensus.

In addition, we show that spin glasses on scale-free networks seem to obey universality. This means that, in the pure spin-glass case, the type of the interaction does not seem to affect the nature of the order when opinion forms. Furthermore, for $\lambda > 4$ [15] spin glasses on scale-free networks have the same universality class as the mean-field Sherrington-Kirkpatrick [19] Ising spin glass [20].

In Sec. II we introduce the Hamiltonian studied, followed by how the networks are constructed in Sec. III. In Sec. IV we present analytical results and construct a λ–p (network strength versus fraction of ferromagnetic bonds) phase diagram. Details about the simulations are shown in Sec. V, followed by numerical results in Sec. VI and concluding remarks.

II. MODEL

The Hamiltonian of the Edwards-Anderson Ising spin glass [21, 22] defined on a scale-free graph is given by

$$\mathcal{H}(\{s_i\}) = -\sum_{i<j}^{N} J_{ij}\varepsilon_{ij}s_i\,s_j, \tag{2}$$

where the Ising spins $s_i \in \{\pm 1\}$ lie on a scale-free graph with N sites and interactions

$$\mathcal{P}(J_{ij},\varepsilon_{ij}) = \wp_J(J_{ij})\left[\left(1-\frac{\kappa}{N}\right)\delta(\varepsilon_{ij}) + \frac{\kappa}{N}\delta(\varepsilon_{ij}-1)\right]. \tag{3}$$

In Eq. (3) $\varepsilon_{ij} = 1$ if a bond is present between spin s_i and s_j and $\varepsilon_{ij} = 0$ otherwise. κ denotes the mean connectivity of the underlying graph. The connectivity of site i,

$k_i := \sum_j \varepsilon_{ij}$, is sampled from the scale-free distribution, Eq. (1). The bond values are drawn from either a Gaussian distribution with zero mean and standard deviation unity, that is,

$$\wp_J(J_{ij}) \sim \exp\left(-J_{ij}^2/2\right) \tag{4}$$

or a bimodal distribution defined via

$$\wp_J(J_{ij}) = (1-p)\delta(J_{ij}+1) + p\delta(J_{ij}-1)\,. \tag{5}$$

In Sec. III we describe in detail how the scale-free graphs as shown in Fig. 1 are generated for the simulations.

III. GENERATING SCALE-FREE GRAPHS

One standard approach for the generation of scale-free networks is preferential attachment [23]. In this physically inspired growth process, a new node is added to the graph at each step, and the probability of attaching to previously existing nodes depends on their edge degrees. This is believed to mimic the creation of scale-free networks in a wide variety of processes, where newcomers are more likely to associate with already-popular members of the network. The frustration that must be present for the disordered problem to be nontrivial requires that there be loops present in the network. The new nodes must therefore attach to multiple pre-existing nodes in this particular growth process. The simplest implementation of preferential attachment, where the probability of attaching to a node of edge degree k is proportional to k produces a power-law distribution of edge degrees with exponent $\lambda = 3$. It is possible to modify the exponent, at least in the $N \to \infty$ limit, by changing the function giving the probability of attachment [24, 25].

Another technique for generating scale-free networks is to extend the classical "configuration model" [26–28]. Here, an edge degree distribution is chosen according to a power law of exponent λ and a graph is chosen randomly from the ensemble of all possible graphs consistent with the chosen edge degree distribution. The chosen graph is then fixed in time for a given sample (i.e., it is a quenched random graph). The procedure for generating the graphs starts by assigning k stubs for each node, where k is drawn from the distribution $\wp_k$ [Eq. (1)], and randomly pairing the stubs. These pairings make up the edges in the graph. If the resulting graph is valid (in our case, we do not allow double edges, and only connected graphs are considered), then it is accepted and may be used for simulation.

In practice, we use a slightly different approach which is much faster but is known to cause the selection of graphs to be slightly nonuniform [29, 30]. If, during the pairing process, a connection is to be made between two stubs corresponding to the same node, this is not allowed. In the method described above, all edges are removed and the pairing starts from the beginning. Here, we simply reject the pairing and move on. This is not expected to affect our results significantly: The degree distribution is fixed independently of this method. In practice, the preferential attachment graphs are quite different than these random graphs, yet our tests give qualitatively similar results for the two cases. The results presented in this paper are from simulations using the quenched random graphs as defined above.

The graph-generation technique used in our simulations works for general degree distributions, although the acceptance rate may be prohibitively low for some graphs. For application to scale-free graphs, an upper bound is imposed on the allowed edge degrees, $k_{\max} = \sqrt{N}$. Although we can generate graphs with k exceeding $\sqrt{N}$, the ensemble is poorly defined in this case: Even randomly chosen graphs cannot be uncorrelated [28, 31, 32]. We also set a lower bound on the edge degree $k_{\min} = 3$. This eliminates spins which could be easily integrated out of the system and do not contribute to the frustration properties: dangling spins with only one attachment, and (possibly long) loops of spins which are not connected with any other spins.

IV. ANALYTICAL RESULTS

Analytical results for spin glasses on scale-free networks were obtained previously [15], and here we adapt a calculation for the Ising ferromagnet on a scale-free graph to the spin-glass case [18].

A. Replica approach

We use the replica approach and at first consider the disorder average of the replicated partition function Z^n for integer powers of n

$$\begin{aligned}\langle\!\langle Z^n \rangle\!\rangle &= \left\langle\!\!\left\langle \sum_{\{s_i^a\}} \exp\left(-\beta \sum_{a=1}^{n} \mathcal{H}(\{s_i^a\})\right)\right\rangle\!\!\right\rangle \\ &= \int \prod_{i<j} \frac{dJ_{ij}\,d\varepsilon_{ij}}{\mathcal{N}} P(J_{ij},\varepsilon_{ij}) \prod_{j=1}^{N} \delta\Big(\sum_{j(\neq i)} \varepsilon_{ij} - k_j\Big) Z^n\,.\end{aligned} \tag{6}$$

The double angular brackets $\langle\!\langle \cdots \rangle\!\rangle$ denote an average only over the quenched interaction variables J_{ij} and ε_{ij}. At the moment the connectivities k_i are fixed. The constraints on these quantities, which are necessary to impose a scale-free degree distribution, will be introduced later [see Eq. (10)] as done byt the authors of Ref. [18]. In Eq. (6) $\mathcal{N}$ is a normalization constant and $\beta = 1/T$ the inverse temperature. After an appropriate continuation to small values of n the expression in Eq. (6) is related to the free energy F of the model via

$$\beta F = -\lim_{n\to 0} \frac{\langle\!\langle Z^n \rangle\!\rangle - 1}{n}\,. \tag{7}$$

Using a representation of the δ-function, the integrals in Eq. (6) factorize resulting in

$$\langle\!\langle Z^n \rangle\!\rangle = \sum_{\{\vec{s}_i\}} \frac{e^{-\kappa N/2}}{\mathcal{N}} \int \prod_i \left(\frac{d\psi_i}{2\pi}\right) \exp\left(-i\sum_{i=1}^{N}\psi_i k_i\right) \times \exp\left[\frac{\kappa}{2N}\sum_{ij}\left\langle e^{\beta J \vec{s}_i\cdot\vec{s}_j}\right\rangle_J e^{i\psi_i}e^{i\psi_j}\right], \quad (8)$$

where $\vec{s}_i$ is an Ising spin with n components. The order parameters

$$\rho(\vec{\sigma}) = \frac{1}{N}\sum_i \delta(\vec{\sigma},\vec{s}_i)e^{i\psi_i}, \quad (9)$$

and their conjugated fields $\hat{\rho}(\vec{\sigma})$ allow one to perform the trace over the spin variables $\vec{s}_i$ in Eq. (8). After replacing the connectivity-dependent site averages with the appropriate averages over the degree distribution $\wp_k$ we obtain

$$\begin{aligned}\frac{1}{N}\sum_{i=1}^{N}\log\sum_{\vec{\sigma}}(\hat{\rho}(\vec{\sigma}))^{k_i} &\equiv \sum_k \wp_k \log\sum_{\vec{\sigma}}(\hat{\rho}(\vec{\sigma}))^k \\ &= \beta f_\lambda(\hat{\rho}). \end{aligned} \quad (10)$$

The partition function $\langle\!\langle Z^n \rangle\!\rangle$ then acquires the form

$$\langle\!\langle Z^n \rangle\!\rangle \propto \int \prod_{\vec{\sigma}} d\rho(\vec{\sigma}) d\hat{\rho}(\vec{\sigma}) \exp\Big(-N\beta f_{\rm trial}(\rho,\hat{\rho})\Big) \quad (11)$$

with the trial free energy

$$\begin{aligned}\beta f_{\rm trial}(\rho,\hat{\rho}) &= \kappa\sum_{\vec{\sigma}}\rho(\vec{\sigma})\hat{\rho}(\vec{\sigma}) + \frac{\kappa}{2} - \beta f_\lambda(\hat{\rho}) \\ &\quad -\frac{\kappa}{2}\sum_{\vec{\sigma},\vec{\tau}}\rho(\vec{\sigma})\rho(\vec{\tau})\left\langle e^{\beta J(\vec{\sigma},\vec{\tau})}\right\rangle_J, \end{aligned} \quad (12)$$

where the average over the distribution $\wp_J$ is represented as $\langle\cdots\rangle_J$. The integral in Eq. (11) can be evaluated with the method of steepest descent leading to a self-consistent equation for the order parameters ρ:

$$\rho(\vec{\sigma}) = \sum_k \frac{k}{\kappa}\wp_k \left(\sum_{\vec{\tau}}\rho(\vec{\tau})\left\langle e^{\beta J(\vec{\sigma},\vec{\tau})}\right\rangle_J\right)^{k-1}. \quad (13)$$

Finding stable solutions to this equation in the $n\to 0$ limit would lead to the free energy of the model at all temperatures. This problem remains to be solved for general spin-glass Hamiltonians. However, here we are interested *only* in the transition temperature of the system. In this case the simplest replica symmetric analysis is sufficient.

B. Replica-symmetric solution

Due to the Boolean nature of the Ising spins, the replica-symmetric solution $\rho_{\rm rs}(\vec{\sigma})$ of Eq. (13) only depends on the sum $s = \sum_a \sigma_a$ of the components of $\vec{\sigma}$. The parametrization

$$\rho_{\rm rs}(\vec{\sigma}) = \int dh \mathcal{P}(h)\exp(\beta h s), \quad (14)$$

allows one to perform the limit $n\to 0$ straightforwardly, which leads to the self-consistent equation for the local-field distribution

$$\mathcal{P}(h) = \sum_{k=k_{\rm min}}^{\infty}\wp_k\frac{k}{\kappa}\int\prod_{i=1}^{k-1}dh_i dJ_i \mathcal{P}(h_i)\wp_J(J_i) \times\delta\left(h - \sum_{i=1}^{k-1}u(h_i,J_i)\right) \quad (15)$$

with u defined as

$$u(h,J) = \frac{1}{\beta}\text{atanh}[\tanh(\beta h)\tanh(\beta J)]. \quad (16)$$

As pointed out in Ref. [18] and calculated in Ref. [33] this equation can be derived within the cavity framework [34]. When connecting a new site to the system, one has to take into account the heterogeneity of the graph, which is reflected in the distribution $(k/\kappa)\wp_k$ on the right-hand side of Eq. (15). The spin-glass order parameter $q = \langle\!\langle s_i\rangle_T^2\rangle_J$, where $\langle\cdots\rangle_T$ represents a thermal average, is related to the local-field distribution via

$$q = \sum_{k=k_{\rm min}}^{\infty}\wp_k\int\prod_{i=1}^{k}dh_i dJ_i\mathcal{P}(h_i)\wp_J(J_i) \times\tanh^2\left(\beta\sum_{i=1}^{k}u(h_i,J_i)\right), \quad (17)$$

whereas the magnetization $m = \langle\!\langle s_i\rangle_T\rangle_J$ is given by

$$m = \sum_{k=k_{\rm min}}^{\infty}\wp_k\int\prod_{i=1}^{k}dh_i dJ_i\mathcal{P}(h_i)\wp_J(J_i) \times\tanh\left(\beta\sum_{i=1}^{k}u(h_i,J_i)\right). \quad (18)$$

The expressions for the order parameters are derived by using real replicas of the system. Following the notation of Viana and Bray we also introduce the quantities

$$q_n = \int dh\,\mathcal{P}(h)\tanh^n(\beta h), \quad (19)$$

and remind the reader, that the inequality $q_2 \geq q_n$ holds for all even $n > 2$.

The δ-function is always a solution of the self-consistent equation, Eq. (15). Due to the vanishing of all local fields, and consequently of the order parameters m and q, this solution intuitively corresponds to the paramagnetic phase. Based on physical grounds, we expect this solution to be unstable below a critical temperature, which thus signals a transition to a frozen low-temperature phase.

We first test the stability of this paramagnetic solution towards a spin-glass transition. To this end we introduce a distribution $\mathcal{P}_0$ with a small $q_2 = \epsilon$ on the right-hand side of Eq. (15). If the corresponding quantity of the resulting distribution on the left-hand side exceeds ϵ, the paramagnetic solution becomes unstable and the system undergoes a spin-glass transition. The critical temperature $T_c^{\rm SG}$ is given by the equation

$$1 = \sum_k \frac{k(k-1)}{\kappa} \wp_k \left\langle \tanh^2\left(\frac{J}{T_c^{\rm SG}}\right)\right\rangle_J . \qquad (20)$$

To detect a transition towards a ferromagnetic phase a similar procedure using a distribution $\mathcal{P}_0$ with a small $q_1 = \epsilon$ can be applied. This leads to the stability criterion to determine $T_c^{\rm FM}$, that is,

$$1 = \sum_k \frac{k(k-1)}{\kappa} \wp_k \left\langle \tanh\left(\frac{J}{T_c^{\rm FM}}\right)\right\rangle_J . \qquad (21)$$

When lowering the temperature the system enters the frozen phase with the higher T_c. Within the low-temperature phase no conjectures can be made from this "paramagnetic" analysis. Note that the usual procedure to determine T_c (which relies on the moments of the distribution $\mathcal{P}$) fails here for small values of the scale-free decay parameter ($\lambda \leq 4$), because in this region the moments cease to exist.

For a bimodal bond distribution [Eq. (5)] with minimum connectivity $k_{\rm min} = 3$ the solutions of Eqs. (20) and (21) are visualized in Fig. 2. The color represents the value of the critical temperature. The darker the color, the smaller the numerical value. Note that both transition temperatures diverge for $\lambda \leq 3$, because the second moment of the degree distribution is infinite. In the blue-white region (top shaded region of the graph) the system is always ferromagnetic with $T_c^{\rm FM}$ increasing for $\lambda \to 2$. In the red-yellow region (bottom shaded region of the graph) the system is a spin glass at all finite temperatures with $T_c^{\rm SG}$ increasing for $\lambda \to 2$. For the particular case of $p = 0.5$ $T_c^{\rm SG} \to \infty$ for $\lambda \leq 3$ and $T_c^{\rm SG}$ finite for $\lambda > 3$.

C. Comparison to the static model

We briefly compare our result to previous calculations. In the work of Kim *et al.* [15] the "static" model was used. In this approach a probability $\pi_i \propto i^{-\mu}$, $\mu \in [0,1)$ is assigned to each vertex $i = 1, \ldots, N$ to obtain a scale-free graph with degree $\lambda = 1 + \mu^{-1}$ and mean connectivity κ. The results derived for the phase boundaries in Ref. [15] rely on a *truncation scheme* which confines the number of the order parameters to the "most important" ones [35]. At the replica-symmetric level, this approximation is equivalent to the assumption of Gaussian local fields, which can be avoided, using a variant of the approach described above.

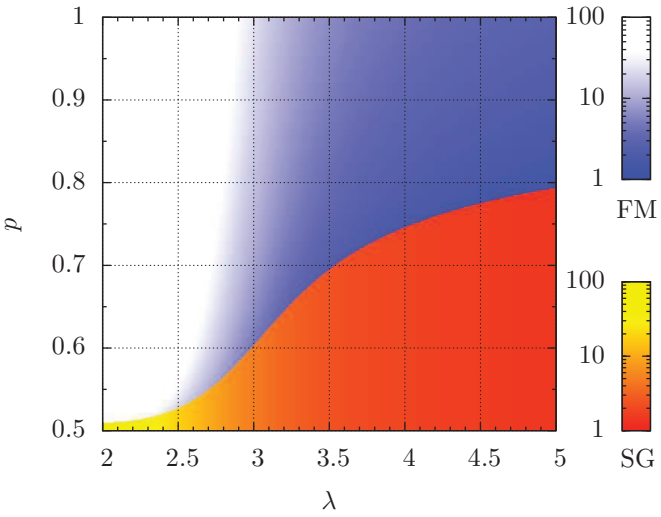

FIG. 2: (Color online) Analytical phase diagram: Fraction of ferromagnetic bonds p vs exponent λ. Color represents the value of the critical temperature. The darker the color, the smaller the numerical value. For $\lambda \leq 3$, both $T_c^{\rm FM}$ and $T_c^{\rm SG}$ diverge, but there is a crossover in the rates at which they diverge. In this case, in the blue-white region (top shaded region of the graph) the system is ferromagnetic at all finite temperatures, while in the red-yellow region (bottom shaded region of the graph), the system is a spin glass at all finite temperatures. Note that for $\lambda \to 2$ the system becomes increasingly stable against local (temperature) perturbations. For the particular case of $p = 0.5$ (horizontal axis) $T_c^{\rm SG} \to \infty$ for $\lambda \leq 3$ and $T_c^{\rm SG}$ finite for $\lambda > 3$.

Starting from Eq. (10) in Ref. [15] we proceed using the order parameters

$$\rho(\vec{\sigma}) = \frac{1}{N}\sum_i \pi_i \delta(\vec{\sigma}, \vec{s}_i) \qquad (22)$$

and their conjugated variables $\hat{\rho}(\vec{\sigma})$. The functions which still depend on the vertex weights π_i can be transformed to integrals in the thermodynamic limit according to

$$\frac{1}{N}\sum_{i=1}^{N} g(\kappa N \pi_i) \approx \int_0^1 dx g\left((1-\mu)\frac{\kappa}{x^\mu}\right) = \int_{k_{\rm min}}^{\infty} dk\, \wp(k) g(k) .$$

In the last step we performed a substitution which directly leads to the scale-free distribution relevant for the static model

$$\wp(k) \;=\; \left(k_{\rm min}\right)^{\lambda-1} \frac{\lambda-1}{k^\lambda}, \quad k_{\rm min} = \frac{\lambda-2}{\lambda-1}\kappa . \qquad (23)$$

The partition function $\langle\langle Z^n \rangle\rangle$ of the static model reduces to a saddle-point integral [see Eq. (11)] with a scale-free dependent part in the the trial free energy (12):

$$\beta f_\lambda(\hat{\rho}) \;=\; \int_{k_{\rm min}}^{\infty} dk\, \wp(k) \log\left[\sum_{\vec{\sigma}} \exp\left(k\hat{\rho}(\vec{\sigma})\right)\right] .$$

Using the saddle-point equations and the replica-symmetric Ansatz, we obtain a self-consistent equation for the distribution of local fields

$$\mathcal{P}(h) = \int_{k_{\min}}^{\infty} dk\, \wp(k) \frac{k}{\kappa} \sum_{m=0}^{\infty} \frac{e^{-k} k^m}{m!} \int \prod_{i=1}^{m} dh_i dJ_i \times \mathcal{P}(h_i) \wp_J(J_i) \delta\left(h - \sum_i^m u(h_i, J_i)\right). \quad (24)$$

This equation is a generalization of the replica-symmetric equations for the Viana-Bray model [35, 36] where the mean connectivity k is sampled from the distribution $(k/\kappa)\wp(k)$. Moreover, the equation is similar to the self-consistent equation [Eq. (15)], where the connectivities are sampled from the distribution $(k/\kappa)\wp_k$. This last approach is a generalization of the fixed-connectivity model to arbitrary degree distributions, and we prefer it due to its generality. The paramagnetic solution $\mathcal{P}(\cdot) = \delta(\cdot)$ is a solution of Eq. (24) which becomes unstable towards a spin-glass transition at the critical temperature T_c^{SG}

$$1 = \left\langle \tanh^2\left(\frac{J}{T_c^{\mathrm{SG}}}\right)\right\rangle_J \int_{k_{\min}}^{\infty} dk\, \wp(k) \frac{k^2}{\kappa} = \kappa \left\langle \tanh^2\left(\frac{J}{T_c^{\mathrm{SG}}}\right)\right\rangle_J \frac{(\lambda-2)^2}{(\lambda-1)(\lambda-3)}. \quad (25)$$

The transition to a ferromagnetic phase occurs at the critical temperature T_c^{FM}

$$1 = \kappa \left\langle \tanh\left(\frac{J}{T_c^{\mathrm{FM}}}\right)\right\rangle_J \frac{(\lambda-2)^2}{(\lambda-1)(\lambda-3)}. \quad (26)$$

In the last line of Eq. (25) we performed the integrals which are convergent for $\lambda > 3$ *only*. This representation coincides with the predictions for the critical temperature in Ref. [15]. Here the results were obtained *without resorting to a truncation scheme*. Predictions for the de Almeida Thouless line [37] relying on Gaussian approximations [38] can lead to results which were shown to be wrong [39, 40]. The investigation of the phase boundaries in the presence of an external magnetic field seems promising in this approach, and will be reported elsewhere.

D. Critical exponents

We now turn to the computation of the critical exponent which governs the growth of the order parameter close to the transition temperature. The order parameter is proportional to τ^β, here τ is the reduced temperature (i.e., $\tau = 1 - T/T_c$ and β a critical exponent).

Note that close to T_c all q_n are small, as $\mathcal{P}$ is close to a δ function. This allows us to neglect q_n with large n in this region while keeping the dominant terms (i.e., q_2 for the spin-glass transition and q_1 for the ferromagnetic transition). In particular, close to T_c the order parameters q and m are proportional to q_2 and q_1, respectively. It is therefore sufficient to investigate how these quantities evolve from zero below T_c.

We start with the spin-glass transition and derive a self-consistent equation for q_2:

$$q_2 \approx \sum_k \wp_k \frac{k}{\kappa} \sum_{l=1}^{k-1} t_l \binom{k-1}{l} q_2^l \langle \tanh^2(\beta J)\rangle_J^l, \quad (27)$$

where t_l are Taylor coefficients of $\tanh^2$. To obtain Eq. (27) we use the self-consistent equation [Eq. (15)] for $\mathcal{P}$ and employ a series expansion in terms of the $\{\tanh(\beta h_i)\tanh(\beta J_i)\}$. We then evaluate all averages with respect to $\mathcal{P}$ and $\wp_J$ and finally perform the aforementioned approximation (i.e., neglect all q_n with $n > 2$).

If $\lambda > 4$ we recover the Sherrington-Kirkpatrick mean-field critical exponents by truncating the second sum after the $l = 2$ contribution on the right hand side of the equation, which amounts to

$$q \propto \frac{1 - \langle k(k-1)\rangle_k \kappa^{-1} \left\langle \tanh^2(\beta J)\right\rangle_J}{\langle k(k-1)(k-2)\rangle_k \left\langle \tanh^2(\beta J)\right\rangle_J^2} \propto \tau + \mathcal{O}(\tau^2),$$

that is,

$$\beta = 1, \qquad (\lambda > 4). \quad (28)$$

For $\lambda \leq 4$ the k average in the denominator of the last equation diverges and the usual technique to extract the critical exponent does not work.

For $\lambda \leq 4$ we note that due to the combinatorial factor in Eq. (27) the lower (important) powers l of q have a prefactor proportional to k^l, such that the divergent part ($l \geq 2$) depends on the combination $kq_2 \left\langle \tanh^2(\beta J)\right\rangle_J$ only. We assume that this is the important k dependence and introduce a function F in the following way:

$$\begin{aligned} &\sum_k \wp_k \frac{k}{\kappa} \sum_{l=2}^{k-1} t_l \binom{k-1}{l} q_2^l \left\langle \tanh^2(\beta J)\right\rangle_J^l \\ &\quad \approx \sum_k \wp_k \frac{k}{\kappa} F\left(k q_2 \left\langle \tanh^2(\beta J)\right\rangle_J\right) \\ &\quad \approx \int_{k_{\min}}^{\infty} dk \frac{c}{\kappa} \frac{1}{k^{\lambda-1}} F\left(k q_2 \left\langle \tanh^2(\beta J)\right\rangle_J\right) \\ &\quad \approx \left(q_2 \left\langle \tanh^2(\beta J)\right\rangle_J\right)^{\lambda-2} \int_{x_{\min}}^{\infty} dx \frac{c}{\kappa} \frac{1}{x^{\lambda-1}} F(x). \end{aligned}$$

In the last line we scaled out q_2 by a substitution leading to the lower integration bound $x_{\min} = q_2 \left\langle \tanh^2(\beta J)\right\rangle_J k_{\min}$. The quadratic dependence of F at the origin due to the fact that the series expansion starts with $l = 2$ allows one to put $x_{\min} \propto q_2 \to 0$ for $\lambda < 4$. Inserting the above steps into Eq. (27) we obtain

$$q^{\lambda-3} \propto \frac{1 - \langle k(k-1)\rangle_k \kappa^{-1} \left\langle \tanh^2(\beta J)\right\rangle_J}{\left\langle \tanh^2(\beta J)\right\rangle_J^{\lambda-2} \int_0^{\infty} dx \frac{c}{\kappa} \frac{1}{x^{\lambda-1}} F(x)} \propto \tau + \mathcal{O}(\tau^2).$$

This means

$$\beta = 1/(\lambda - 3), \qquad (3 < \lambda < 4), \tag{29}$$

which agrees with the result of Kim *et al.* [15] derived within the static approximation. The limiting case $\lambda = 4$ needs some special care, leading to logarithmic corrections [i.e., $q \propto -\tau/\log(\tau)$].

To reproduce the results for the critical exponent in the ferromagnetic sector, which were calculated by the authors of Ref. [18], the same technique can be used. In particular

$$\beta = 1/2, \qquad (\lambda > 5). \tag{30}$$

This means the system is in the mean-field universality class for $\lambda > 5$ because, within $\mathcal{O}(\tau^2)$

$$m^2 \propto \frac{1 - \langle k(k-1)\rangle_k \kappa^{-1} \langle \tanh(\beta J)\rangle_J}{\langle k(k-1)(k-2)(k-3)\rangle_k \langle \tanh(\beta J)\rangle_J^3} \propto \tau + \dots .$$

For $\lambda \leq 5$ we face the same problem as in the spin-glass sector when $\lambda \leq 4$, because the k average in the denominator diverges. Performing analogous considerations leads to

$$\beta = 1/(\lambda - 3), \qquad (3 < \lambda < 5). \tag{31}$$

Finally, for $\lambda = 5$, $m^2 \propto -\tau/\log(\tau)$.

Summarizing, for $\lambda > 4$ [$\lambda > 5$] in the SG [FM] sector, the critical exponents agree with the mean-field case, whereas for $3 < \lambda < 4$ [$3 < \lambda < 5$] in the SG [FM] sector the critical exponents depend on the exponent λ.

V. NUMERICAL DETAILS

We validate the aforementioned analytical results using Monte Carlo simulations. In particular, the numerical results show the strength of the different corrections to scaling depending on the choice of the exponent λ of the scale-free network.

A. Observables

To determine the location of both the ferromagnetic and spin-glass phase transitions we measure first the Binder cumulant [41] defined via

$$g = \frac{1}{2}\left(3 - \frac{\langle\!\langle\!\langle \mathcal{O}^4 \rangle\!\rangle\!\rangle}{\langle\!\langle\!\langle \mathcal{O}^2 \rangle\!\rangle\!\rangle^2}\right) . \tag{32}$$

In Eq. (32), $\langle\!\langle\!\langle \cdots \rangle\!\rangle\!\rangle$ represents an average over the disorder via $\langle \cdots \rangle_J$, the random graphs via $\langle \cdots \rangle_k$, and Monte Carlo time (i.e., $\langle \cdots \rangle_T$). Furthermore, $\mathcal{O}$ is either the magnetization m in the ferromagnetic sector defined via

$$m = \frac{1}{N}\sum_i s_i \tag{33}$$

or the spin-glass overlap q in the spin-glass sector given by

$$q = \frac{1}{N}\sum_{i=1}^{N} s_i^\alpha s_i^\beta . \tag{34}$$

In Eq. (34), "α" and "β" represent two copies of the system with the same disorder. The Binder ratio is dimensionless and thus has the simple scaling form

$$g = \widetilde{G}\left(N^{1/\nu}[T - T_c]\right) , \tag{35}$$

where T_c represents the transition temperature. The expression in Eq. (35) is valid in the non-mean-field region (i.e., for $\lambda < 4$ in the spin-glass sector and $\lambda < 5$ in the ferromagnetic sector [15]). In the spin-glass mean-field region ($\lambda > 4$) Eq. (35) is replaced by [42]

$$g = \widetilde{G}\left(N^{1/3}[T - T_c]\right) . \tag{36}$$

Note that the two-point finite-size correlation length [43–46] typically used to pinpoint transitions in glassy systems cannot be used here because the spins are placed on a lattice that has no geometry.

The calculation of the Binder ratio g allows one to determine T_c and the critical exponent ν for both the spin-glass and ferromagnetic sectors. However, to fully characterize the critical behavior of the model, a second critical exponent has to be computed [5]. We have also computed the susceptibility χ given by

$$\chi = N\langle\!\langle\!\langle \mathcal{O}^2 \rangle\!\rangle\!\rangle . \tag{37}$$

In the ferromagnetic case we therefore measure

$$\chi_m = N\langle\!\langle\!\langle m^2 \rangle\!\rangle\!\rangle \tag{38}$$

with the magnetization m given by Eq. (33), whereas in the spin-glass case we measure

$$\chi_q = N\langle\!\langle\!\langle q^2 \rangle\!\rangle\!\rangle \tag{39}$$

with the spin-glass overlap q defined in Eq. (34). In general, the scaling behavior of the susceptibility is given by

$$\chi = N^{2-\eta}\widetilde{C}\left(N^{1/\nu}[T - T_c]\right) , \tag{40}$$

where a simple finite-size scaling yields the exponent η. Unfortunately, fluctuations in the data are huge and thus the determination of the critical exponent η is not possible. However, in the mean-field regime, the finite-size scaling form presented in Eq. (40) is replaced by

$$\chi = N^{1/3}\widetilde{C}\left(N^{1/3}[T - T_c]\right) . \tag{41}$$

Therefore, curves of $\chi/N^{1/3}$ should have the same scaling behavior as the Binder ratio [Eq.(36)]: When $T = T_c$ data for different system sizes cross at a point (up to scaling corrections).

B. Equilibration and simulation parameters

The simulations are done using the parallel tempering Monte Carlo method [47]. For the pure spin glass we first simulate the system with Gaussian disorder to obtain an idea of the equilibration behavior when the Ising model with disorder is defined on a scale-free graph. Furthermore, in the Gaussian case we can perform a rigorous equilibration test [48, 49] where the energy per spin $[U = (1/N)\langle\langle\langle\mathcal{H}\rangle\rangle\rangle$ with $\mathcal{H}$ defined in Eq. (2)] is compared to an expression derived from the link overlap q_4 [defined below in Eq. (42)]. The data for both the energy per spin U and the energy per spin computed from the link overlap,

$$U(q_4) = -\frac{1}{T}\left\langle\!\!\left\langle\!\!\left\langle \frac{N_b}{N}\,(1-q_4)\right\rangle\!\!\right\rangle\!\!\right\rangle\,, \tag{42}$$

where

$$q_4 = \frac{1}{N_b}\sum_{i,j}\varepsilon_{ij}s_i^\alpha s_j^\alpha s_i^\beta s_j^\beta\,, \tag{43}$$

have to coincide when the system is in thermal equilibrium. In Eqs. (42) and (43) N_b is the number of nonzero bonds of a given sample. Note that the expression in Eq. (42) is valid for the spin-glass sector, however, it represents a conservative bound for the ferromagnetic sector [48]. Furthermore, N_b is *inside* the disorder average because the number of bonds fluctuates from sample to sample. Sample data are shown in Fig. 3. Once $U = U(q_4)$ the data for the squared order parameter q^2 (shifted for better viewing in Fig. 3) are also in thermal equilibrium.

For the bimodal disorder distribution and the ferromagnetic sector the aforementioned equilibration test cannot be used. In this case we preform a logarithmic binning of all observables. Once the data for the last three bins agree within error bars we deem the system to be in thermal equilibrium. The simulation parameters are shown in Table I.

VI. NUMERICAL RESULTS

We first study Gaussian disorder where we have a strong equilibration test to ensure that the data are in thermal equilibrium. Corrections to scaling are very large for this model despite the large number of samples studied.

A. Gaussian disorder

Figure 4 shows data for the Binder ratio g_q for Gaussian disorder and $\lambda = 3.0$, right at the onset (see Fig. 2) where the critical temperature for the spin-glass (SG) sector starts to diverge. The crossing temperatures between lines for $N/2N$ pairs grow with the system size

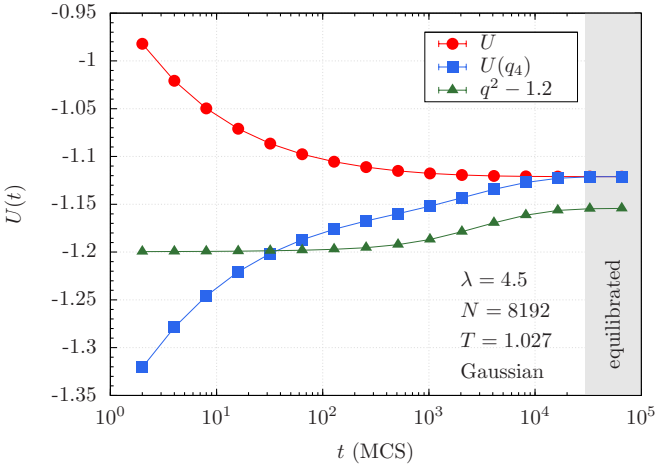

FIG. 3: (Color online) Example equilibration plot for Gaussian disorder for $N = 8192$ spins at $T = 1.027$ (lowest temperature simulated) and $\lambda = 4.5$. Once the data for the energy U and the energy computed from q_4 $[U(q_4)]$ agree, the system is in thermal equilibrium. This can be seen also with data for q^2 that also are independent of Monte Carlo time. Note that the data for q^2 are shifted by 1.2 for better viewing. Error bars are smaller than the symbols.

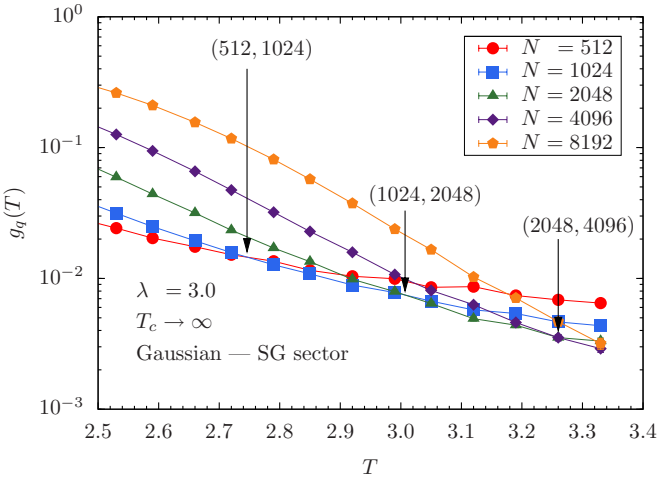

FIG. 4: (Color online) Binder ratio g_q for the SG sector and $\lambda = 3.0$ with Gaussian disorder for different system sizes N. The crossings between increasing system-size pairs diverge with increasing system size suggesting that $T_c^{\rm SG} \to \infty$, in agreement with the analytical predictions.

in agreement with the analytic calculations. To prevent $T_c^{\rm SG}$ for the SG sector to diverge, the bonds would have to be re-scaled. Furthermore, there is no transition in the ferromagnetic sector (not shown), in agreement with the analytical calculations.

In Fig. 5 we show data for $\lambda = 3.5$. In agreement with the analytical predictions $T_c^{\rm SG}$ is finite, albeit with huge corrections to scaling. We estimate $T_c^{\rm SG} = 2.31(3)$. Note that this estimate is computed via a finite-size scaling of the data and only takes statistical fluctuations into ac-

TABLE I: Parameters of the simulation: For each exponent λ, system size N and fraction of ferromagnetic bonds p (note: Gaussian disorder is marked with "Gauss") we compute $N_{\rm sa}$ disorder or network instances. $N_{\rm sw} = 2^b$ is the total number of Monte Carlo sweeps for each of the $2N_T$ replicas for a single instance, $T_{\rm min}$ [$T_{\rm max}$] is the lowest [highest] temperature simulated, and N_T is the number of temperatures used in the parallel tempering method for each system size N.

λ	p	N	$N_{\rm sa}$	b	$T_{\rm min}$	$T_{\rm max}$	N_T
3.0	0.500	1024	10 000	15	2.011	4.208	37
3.0	0.500	2048	9 940	15	2.011	4.208	37
3.0	0.500	4096	12 877	17	2.011	4.208	37
3.0	0.500	8192	5 399	19	2.011	4.208	37
3.5	0.500	1024	20 416	15	2.011	4.208	37
3.5	0.500	2048	10 396	15	2.011	4.208	37
3.5	0.500	4096	18 683	17	2.011	4.208	37
3.5	0.500	8192	12 382	19	2.011	4.208	37
4.5	0.500	1024	9 600	16	1.027	2.410	27
4.5	0.500	2048	9 600	16	1.027	2.410	27
4.5	0.500	4096	9 439	19	1.027	2.410	27
4.5	0.500	8192	9 870	19	1.027	2.410	27
4.5	0.700	1024	9 600	16	1.170	3.949	49
4.5	0.700	2048	8 723	16	1.170	3.949	49
4.5	0.700	4096	10 714	16	1.170	3.949	49
4.5	0.700	8192	8 184	17	1.170	3.949	49
4.5	0.850	1024	13 914	16	1.170	3.949	49
4.5	0.850	2048	12 103	16	1.170	3.949	49
4.5	0.850	4096	9 570	16	1.170	3.949	49
4.5	0.850	8192	7 621	17	1.170	3.949	49
3.0	Gauss	1024	24 352	14	2.340	3.330	16
3.0	Gauss	2048	12 956	14	2.340	3.330	16
3.0	Gauss	4096	13 039	14	2.340	3.330	16
3.0	Gauss	8192	7 987	14	2.340	3.330	16
3.5	Gauss	1024	11 697	14	1.755	3.260	25
3.5	Gauss	2048	19 776	14	1.755	3.260	25
3.5	Gauss	4096	9 367	15	1.755	3.260	25
3.5	Gauss	8192	10 192	16	1.755	3.260	25
4.5	Gauss	1024	13 673	16	1.027	2.410	27
4.5	Gauss	2048	10 224	16	1.027	2.410	27
4.5	Gauss	4096	4 656	16	1.027	2.410	27
4.5	Gauss	8192	8 618	16	1.027	2.410	27

count. We have no control over finite-size corrections. A crude extrapolation suggests that the critical temperature will likely be larger than the quoted analytical value which we treat as a lower bound. This is a generic problem for the estimates of the critical temperature made in the spin-glass sector. Again, there is no transition in the ferromagnetic sector.

Finally, Fig. 6 shows data for $\lambda = 4.5$. The top panel shows the Binder ratio as a function of temperature. The data cross at $T_c^{\rm SG} = 1.39(1)$. Using Eq. (36) [i.e., fixing "$\nu = 3$" in Eq. (35)] we obtain $T_c^{\rm SG} = 1.385(9)$, which agrees within error bars with the previous estimate. This result is verified by data on the scaled spin-glass susceptibility (bottom panel of Fig. 6) where the data also cross in the same region. A finite-size scaling analysis of $\chi_q/N^{1/3}$ gives $T_c^{\rm SG} = 1.3833(8)$, a value of higher precision than when using the Binder ratio. For all values of λ studied

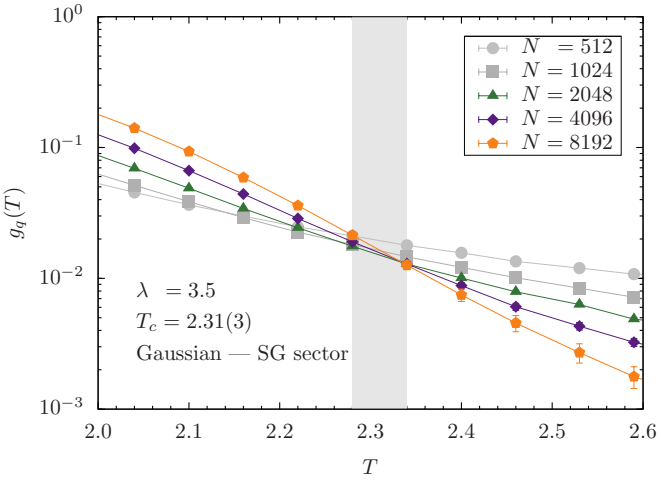

FIG. 5: (Color online) Binder ratio g_q for the SG sector and $\lambda = 3.5$ with Gaussian disorder for different system sizes N. The data show strong corrections to scaling. Using a finite-size scaling analysis we estimate $T_c^{\rm SG} = 2.31(3)$. In this and all subsequent figures, the width of the shaded region around the critical temperature corresponds to the statistical uncertainty for the estimate of the critical temperature using a combination of a finite-size scaling analysis and a bootstrap method.

where $T_c < \infty$ the estimates for the critical exponent ν are listed in Table II. Note that for $\lambda > 4$, "$\nu = 3$" in the scaling form. However, we have allowed for the value to fluctuate when estimating T_c as well.

B. Bimodal disorder

Figure 7 shows data for the Binder ratio g_q for bimodal disorder with $\lambda = 3.0$ and $p = 0.50$. The chosen value of λ is right at the onset (see Fig. 2) where the critical temperature for the spin-glass SG starts to diverge. As for the Gaussian case presented in Sec. VI A, crossing points between lines for $N/2N$ pairs grow with the system size in agreement with the analytic calculations (i.e., $T_c^{\rm SG} \to \infty$). Furthermore, for the FM sector there is no transition (not shown).

In Fig. 8 we show data for $\lambda = 3.5$ and $p = 0.50$. In agreement with the analytical predictions $T_c^{\rm SG}$ is finite, albeit with large corrections to scaling. We estimate $T_c^{\rm SG} = 2.55(8)$. Again, there is no ferromagnetic transition (not shown).

We now study in detail $\lambda = 4.5$ for different concentrations of ferromagnetic bonds p. Figure 9 shows data for the Binder ratio for $\lambda = 4.5$ and $p = 0.50$ for both SG and FM sectors. For the SG sector (top panel), the data cross cleanly at $T_c^{\rm SG} = 1.70(1)$ [1.695(8) when Eq. (36) is used]. The center panel shows data for the scaled spin-glass susceptibility. We obtain $T_c^{\rm SG} = 1.6929(7)$, in agreement with the estimate from the Binder ratio, albeit with higher precision. However, for the FM sector (bottom panel) the data strongly suggest that $T_c^{\rm FM}$ is not

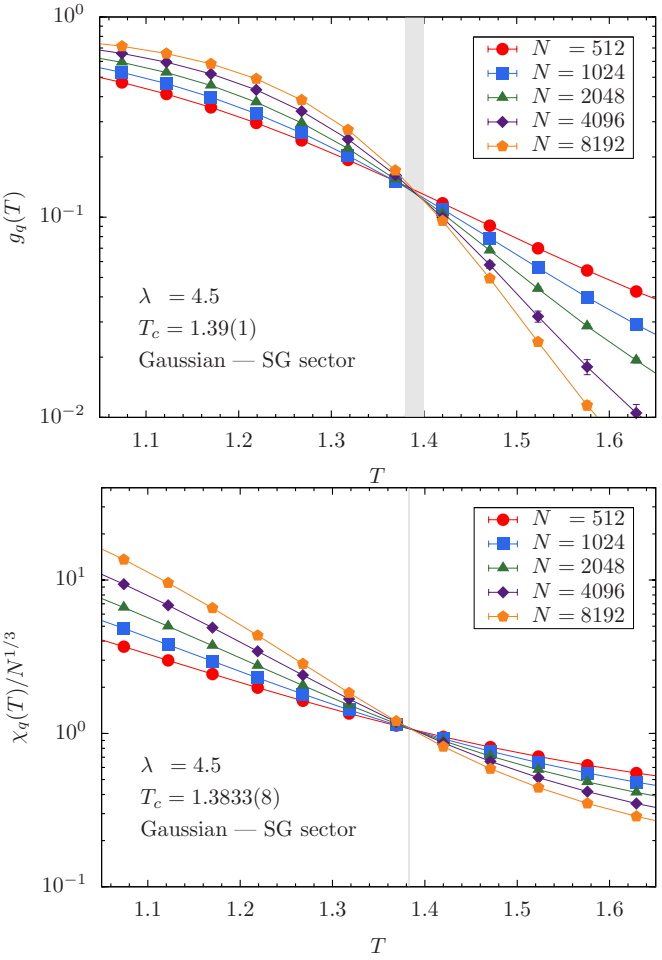

FIG. 6: (Color online) Top: Binder ratio g_q for the SG sector and $\lambda = 4.5$ with Gaussian disorder for different system sizes N. Corrections to scaling are small and we estimate $T_c^{\rm SG} = 1.39(1)$. Using Eq. (36) we obtain $T_c^{\rm SG} = 1.385(9)$, which agrees within error bars with the previous estimate. Bottom: Scaled spin-glass susceptibility $\chi_q/N^{1/3}$ with $\lambda = 4.5$ and Gaussian disorder for different system sizes N as a function of temperature. The data cross at a point (shaded area) and we obtain $T_c^{\rm SG} = 1.3833(8)$.

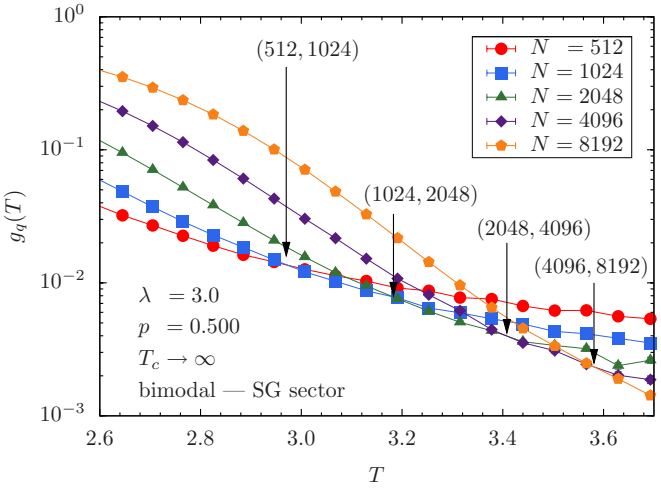

FIG. 7: (Color online) Binder ratio g_q for the SG sector and $\lambda = 3.0$ with bimodal disorder for different system sizes N and $p = 0.50$. As for the Gaussian case (Fig. 4), the crossings between increasing system-size pairs diverge with increasing system size suggesting that $T_c^{\rm SG} \to \infty$, in agreement with the analytical predictions.

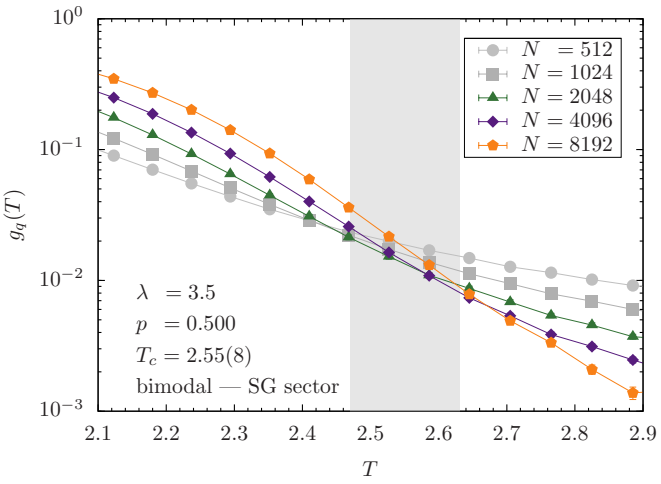

FIG. 8: (Color online) Binder ratio g_q for the SG sector and $\lambda = 3.5$ with bimodal disorder for different system sizes N and $p = 0.50$. As for the Gaussian case (Fig. 5), the data show strong corrections to scaling. Using a finite-size scaling analysis we estimate $T_c^{\rm SG} = 2.55(8)$.

defined, in agreement with the analytic predictions. For $\lambda = 4.5$ the phase boundary between the FM and the SG sector lies somewhere between $p = 0.7$ and 0.85, see Fig. 2. Therefore, we expect that for $p = 0.7$ we only have SG order, whereas for $p = 0.85$ the system orders ferromagnetically.

The case for $p = 0.70$ is shown in Fig. 10. Like for $p = 0.50$, the data for the SG sector show a clear transition, whereas the data for the FM sector suggest that there is no transition. Note that the estimates for $T_c^{\rm SG}$ agree within error bars with the estimates for $p = 0.50$, suggesting that the phase diagram does not depend on p in the SG regime, in agreement with the analytical calculations. For $p = 0.85$ there is no SG order (not shown, in agreement with the analytical results). Moreover, $T_c^{\rm FM} = 2.428(8)$, see Fig. 11.

C. Universality?

To determine if two systems share the same universality class two *independent* critical exponents need to be computed. However, fluctuations in the data are large and therefore estimating the critical exponent η from a finite-size scaling analysis of the susceptibility is difficult. Even worse, η is not properly defined for mean-field models and only α, β, and γ are available.

As shown above in Sec. IV, as well as the work of Kim *et al.* [15] and Dorogovtsev *et al.* [50], the critical ex-

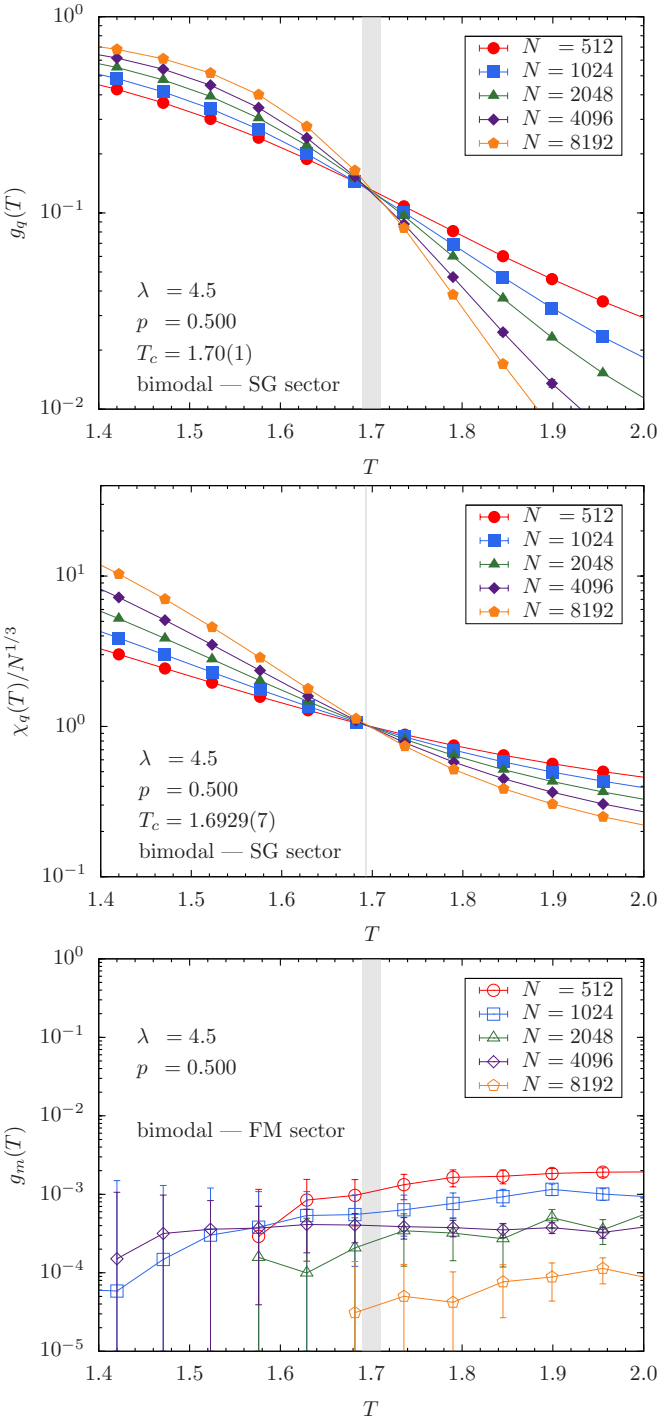

FIG. 9: (Color online) Top panel: Binder ratio g_q for the SG sector and $\lambda = 4.5$ with bimodal disorder ($p = 0.50$) for different system sizes N. We estimate $T_c^{\rm SG} = 1.70(1)$. Using Eq. (36) we obtain $T_c^{\rm SG} = 1.695(8)$, which agrees within error bars with the previous estimate. Center panel: Scaled spin-glass susceptibility $\chi_q/N^{1/3}$ as a function of temperature. The data cross at a point (shaded area) and we obtain $T_c^{\rm SG} = 1.6929(7)$. Bottom panel: Binder ratio g_m for the FM sector. The shaded area in the bottom panel corresponds to $T_c^{\rm SG} = 1.70 \pm 0.01$ (top panel). The data show no sign of ferromagnetic order: The data do not cross and decrease for increasing system size N.

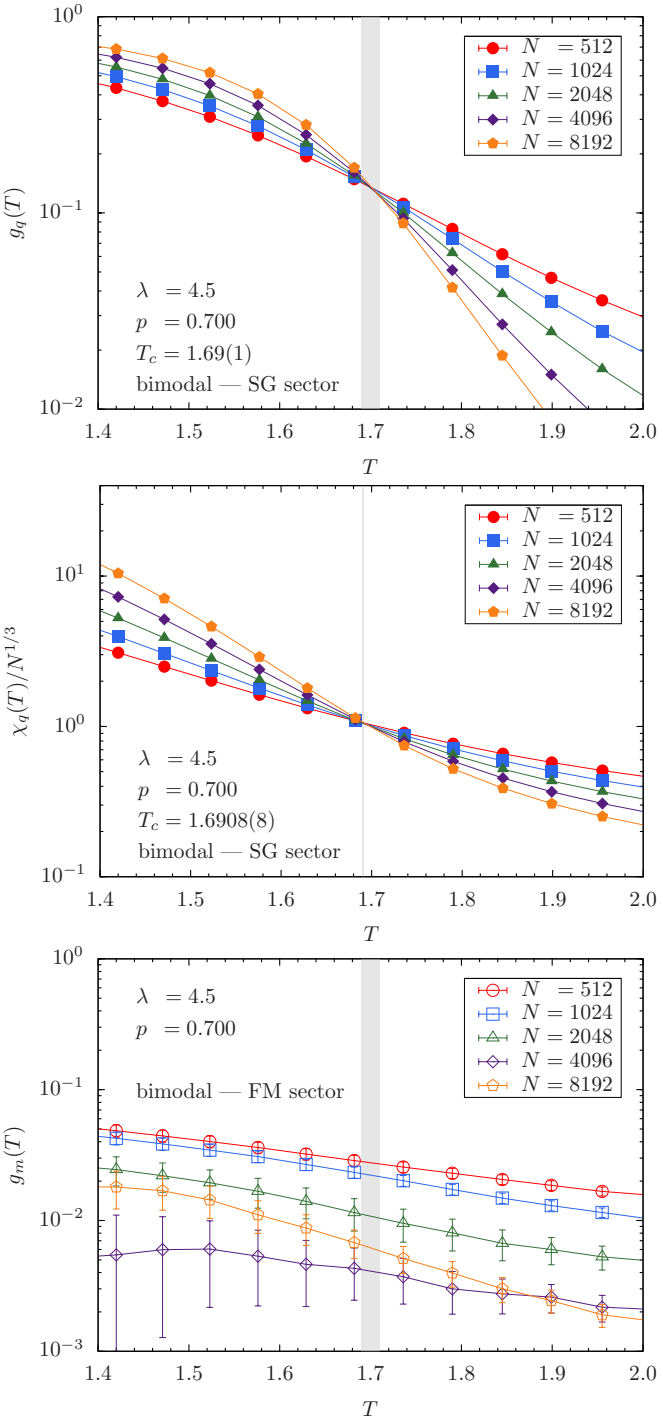

FIG. 10: (Color online) Top panel: Binder ratio g_q for the SG sector and $\lambda = 4.5$ with bimodal disorder ($p = 0.70$) for different system sizes N. We estimate $T_c^{\rm SG} = 1.69(1)$. Using Eq. (36) we obtain $T_c^{\rm SG} = 1.693(9)$, which agrees within error bars with the previous estimate. Center panel: Scaled spin-glass susceptibility $\chi_q/N^{1/3}$ as a function of temperature. The data cross at a point (shaded area) and we obtain $T_c^{\rm SG} = 1.6908(8)$. Bottom panel: Binder ratio g_m for the FM sector. The shaded area in the bottom panel corresponds to $T_c^{\rm SG} = 1.69 \pm 0.01$ (top panel). The data show no sign of ferromagnetic order: The data do not cross and decrease for increasing system size N.

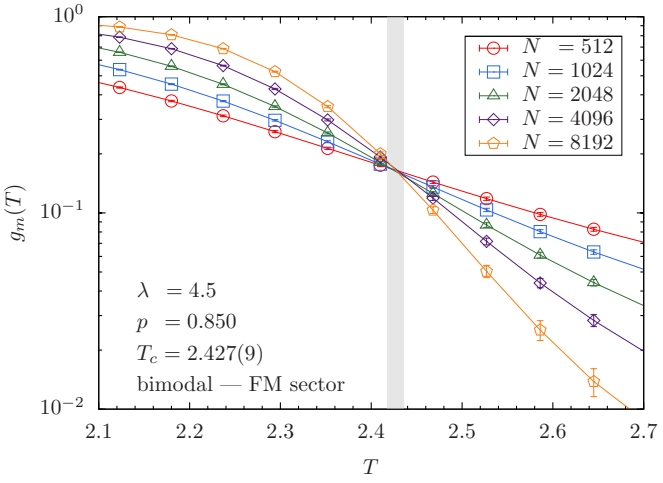

FIG. 11: (Color online) Binder ratio g_m for the FM sector and $p = 0.850$. The shaded area corresponds to $T_c^{\rm FM} = 2.428(8)$. In this case we are deep in the FM sector, the SG sector shows no sign of a transition (not shown).

ponents for spin glasses and ferromagnets on scale-free graphs depend on the exponent λ. In particular, for $\lambda > 4$ the spin-glass sector is predicted to share the same universality class as the mean-field Sherrington-Kirkpatrick model. For $\lambda < 4$ one can show that for the critical exponent β one finds $\beta = \beta(\lambda)$. Similar predictions exist for the ferromagnetic sector where mean-field behavior is recovered for $\lambda > 5$. However, it remains to be determined if the type of disorder (e.g., Gaussian or bimodal) might change the critical exponents.

We compute the critical exponents in an unbiased fashion and with a statistical error bar by letting T_c and $y = 1/\nu$ be parameters. Close to the transition temperature the scaling function can be represented by a third-order polynomial. This is typically a very good approximation. If the optimal values of the critical parameters ν and T_c are chosen, then data for different system sizes should collapse onto a single curve, the scaling function. Therefore, by searching for the optimal fit to a third-order polynomial while minimizing the chi-square of the fit with respect to the critical parameters allows us to determine their optimal values. Statistical error bars to the optimal values are determined by a bootstrap analysis. Note that these error bars take statistical fluctuations into account but cannot properly account for systematic deviations due to corrections to scaling [51].

To test for universality we estimate the critical exponent ν and the value of the dimensionless Binder ratio at T_c [52] (see Table II). Because fluctuations in ν are very large and ν is not properly defined for $\lambda > 4$ (5) in the spin-glass (ferromagnetic) sector we compare in detail $g(T_c)$ in the spin-glass sector. For $\lambda = 3.5$, $g(T_c^{\rm SG}, \lambda = 3.5, \text{Gauss}) = 0.018(3)$, which agrees within error bars with $g(T_c^{\rm SG}, \lambda = 3.5, p = 0.5) = 0.012(25)$. For $\lambda = 4.5$, $g(T_c^{\rm SG}, \lambda = 4.5, \text{Gauss}) = 0.132(12)$, which agrees within error bars with $g(T_c^{\rm SG}, \lambda = 4.5, p = 0.5) = 0.129(12)$. In the bimodal case, we find also that $g(T_c^{\rm SG}, \lambda = 4.5, p = 0.5) = 0.129(12)$ agrees within error bars with $g(T_c^{\rm SG}, \lambda = 4.5, p = 0.7) = 0.136(12)$, thus suggesting the the same universality class might be shared below the spin-glass–to–ferromagnet phase boundary for all values of p. The mean-field Viana-Bray model [35] resembles a fixed-connectivity random graph and is in the same universality class as the Sherrington-Kirkpatrick model. Recent simulations [53] have shown that for the mean-field universality class $g(T_c^{\rm SG}) \approx 0.126(46)$, in agreement with our results for $\lambda > 4$.

TABLE II: Critical parameters T_c [51] and ν, as well as the Binder parameter at the transition temperature $g(T_c^{\rm SG})$, for the spin glass (SG) and ferromagnetic (FM) sectors computed using a finite-size scaling analysis of the data for $N \geq 2048$. Both ν and $g(T_c)$ are universal quantities. This means that if two systems share the same universality class, the values of ν and $g(T_c)$ for both systems should agree. Note that for $\lambda > 4$ we have used the scaling relation from Eq. (35). The obtained exponent $y = 1/\nu$ is compatible with $y = 1/3$ as expected from the mean-field solution. Columns for $\lambda = 4.5$ that state that ν is "fixed" were computed using Eq. (36). Columns for $\lambda = 4.5$ that are marked with a † have estimates of $T_c^{\rm SG}$ computed via a scaling of the susceptibility, Eq. (41).

λ	p	$T_c^{\rm SG}$	$\nu^{\rm SG}$	$g(T_c^{\rm SG})$	$T_c^{\rm FM}$	$\nu^{\rm FM}$
3.0	0.500	∞	—	—	—	—
3.5	0.500	2.55(8)	3.63(79)	0.012(25)	—	—
4.5	0.500	1.70(1)	3.43(51)	0.129(12)	—	—
4.5	0.500	1.695(8)	fixed	0.134(9)	—	—
4.5†	0.500	1.6929(7)	—	—	—	—
4.5	0.700	1.69(1)	3.57(31)	0.136(12)	—	—
4.5	0.700	1.693(9)	fixed	0.144(1)	—	—
4.5†	0.700	1.6908(8)	—	—	—	—
4.5	0.850	—	—	—	2.428(8)	2.70(9)
3.0	Gauss	∞	—	—	—	—
3.5	Gauss	2.31(3)	3.60(25)	0.018(3)	—	—
4.5	Gauss	1.39(1)	3.53(58)	0.132(12)	—	—
4.5	Gauss	1.385(9)	fixed	0.138(9)	—	—
4.5†	Gauss	1.3833(8)	—	—	—	—

Summarizing, our results suggest that for a given value of λ the networks with both Gaussian and bimodal disorder share the *same* universality class. In addition, for values of $\lambda > 4$ the spin-glass sector shares the same universality class as the mean-field Sherrington-Kirkpatrick model.

VII. CONCLUSIONS

We have studied Boolean (Ising) variables on a scale-free graph with competing interactions. Our analytical and numerical results show that for $\lambda \leq 3$ the critical temperature diverges with the system size. For larger values of λ the system undergoes a finite-temperature transition between a spin-glass and a paramagnetic phase. The robustness of both the ferromagnetic and spin-glass

phases suggest that Boolean decision problems on scale-free networks are quite stable to local (temperature) perturbations. For the case with bimodal disorder, we show that for a large enough fraction of ferromagnetic bonds the system orders ferromagnetically at finite temperatures. Finally, for a given value of λ universal critical parameters for both Gaussian and bimodal disorder agree, suggesting universal behavior.

Real networks typically have exponents $\lambda < 3$. It would be interesting to study such a network in the future. Furthermore, the effect of "global biases" (field terms) will also be studied. Finally, opinion formation is an intrinsically nonequilibrium process. For example, what are the temporal patterns of the agents on the networks? What are the effects of time-dependent interactions?

Acknowledgments

We would like to thank Alexander K. Hartmann, M. Niemann, M. Schechter, M. Wittmann and A. P. Young for fruitful discussions. We also thank R. S. Andrist for assistance. H.G.K. acknowledges support from the SNF (Grant No. PP002-114713) and the NSF (Grant No. DMR-1151387). We would like to thank the Texas Advanced Computing Center (TACC) at The University of Texas at Austin for providing HPC resources (Ranger Sun Constellation Linux Cluster), ETH Zurich for CPU time on the Brutus cluster, and Texas A&M University for access to their eos and lonestar clusters.

[1] R. Albert, H. Jeong, and A.-L. Barabási, *Internet: Diameter of the World-Wide Web*, Nature **401**, 130 (1999).
[2] R. Albert and A.-L. Barabási, *Statistical mechanics of complex networks*, Rev. Mod. Phys. **74**, 47 (2002).
[3] http://facebook.com.
[4] http://slashdot.org.
[5] J. M. Yeomans, *Statistical Mechanics of Phase Transitions* (Oxford University Press, Oxford, 1992).
[6] T. Antall, P. L. Krapivsky, and S. Redner, *Social balance on networks: The dynamics of friendship and enmity*, Physica D **224**, 130 (2006).
[7] J. Leskovec, D. Huttenlocher, and J. Kleinberg, in *Proceedings of the 28th ACM Conference on Human Factors in Computing Systems* (2010), p. 1361.
[8] M. Bartolozzi, T. Surungan, D. B. Leinweber, and A. G. Williams, *Spin-glass behavior of the antiferromagnetic Ising model on a scale-free network*, Phys. Rev. B **73**, 224419 (2006).
[9] C. P. Herrero, *Antiferromagnetic Ising model in scale-free networks*, Eur. Phys. J. B **70**, 435 (2009).
[10] M. Weigel and D. Johnston, *Frustration effects in antiferromagnets on planar random graphs*, Phys. Rev. B **76**, 054408 (2007).
[11] Y. Imry and S.-K. Ma, *Random-Field Instability of the Ordered State of Continuous Symmetry*, Phys. Rev. Lett. **35**, 1399 (1975).
[12] J. P. Sethna, K. Dahmen, S. Kartha, J. A. Krumhansl, B. W. Roberts, and J. D. Shore, *Hysteresis and hierarchies: Dynamics of disorder-driven first-order phase transformations*, Phys. Rev. Lett. **70**, 3347 (1993).
[13] S. H. Lee, H. Jeong, and J. D. Noh, *Random field Ising model on networks with inhomogeneous connections*, Phys. Rev. E **74**, 031118 (2006).
[14] J. M. Mooij and H. J. Kappen, *Spin-glass phase transitions on real-world graphs* (2004), (arXiv:cond-mat/0408378).
[15] D.-H. Kim, G. J. Rodgers, B. Kahng, and D. Kim, *Spin-glass phase transition on scale-free networks*, Phys. Rev. E **71**, 056115 (2005).
[16] A. L. Ferreira, J. F. F. Mendes, and M. Ostilli, *First- and second-order phase transitions in Ising models on small-world networks: Simulations and comparison with an effective field theory*, Phys. Rev. E **82**, 011141 (2010).
[17] M. Ostilli, A. L. Ferreira, and J. F. F. Mendes, *Critical behavior and correlations on scale-free small-world networks: Application to network design*, Phys. Rev. E **83**, 061149 (2011).
[18] M. Leone, A. Vázquez, A. Vespignani, and R. Zecchina, *Ferromagnetic ordering in graphs with arbitrary degree distribution*, Eur. Phys. J. B **28**, 191 (2002).
[19] D. Sherrington and S. Kirkpatrick, *Solvable model of a spin glass*, Phys. Rev. Lett. **35**, 1792 (1975).
[20] Note that similar behavior is found in the ferromagnetic sector where the change to the mean-field Ising universality class occurs at $\lambda = 5$ [50].
[21] S. F. Edwards and P. W. Anderson, *Theory of spin glasses*, J. Phys. F: Met. Phys. **5**, 965 (1975).
[22] K. Binder and A. P. Young, *Spin glasses: Experimental facts, theoretical concepts and open questions*, Rev. Mod. Phys. **58**, 801 (1986).
[23] A. L. Barabasi and R. Albert, Science **286**, 509 (1999).
[24] P. L. Krapivsky, S. Redner, and F. Leyvraz, *Connectivity of growing random networks*, Phys. Rev. Lett. **85**, 4629 (2000).
[25] P. L. Krapivsky and S. Redner, *Organization of growing random networks*, Phys. Rev. E **63**, 066123 (2001).
[26] E. A. Bender and E. R. Canfield, *The asymptotic number of labeled graphs with given degree sequences*, J. Comb. Theory A **24**, 296 (1978).
[27] M. E. J. Newman, in *Handbook of Graphs and Networks*, edited by S. Bornholdt and H. G. Schuster (Wiley-VCH, Berlin, 2003).
[28] M. Catanzaro, M. Boguñá, and R. Pastor-Satorras, *Generation of uncorrelated random scale-free networks*, Phys. Rev. E **71**, 027103 (2005).
[29] H. Klein-Hennig and A. K. Hartmann, *Bias in generation of random graphs* (2011), (arxiv:cond-mat/1107.5734).
[30] Note that the method we use to generate the scale-free graphs also suffers from the bias recently characterized by the authors of Ref. [29]. However, for $\lambda \geq 3$, which are the values we are interested in, this has no effect on the data.
[31] Z. Burda and A. Krzywicki, *Uncorrelated random networks*, Phys. Rev. E **67**, 046118 (2003).

[32] M. Boguñá, R. Pastor-Satorras, and A. Vespignani, *Cut-offs and finite size effects in scale-free networks*, Eur. Phys. J. B **38**, 205 (2004).

[33] B. Wemmenhove, T. Nikoletopoulos, and J. P. L. Hatchett, *Replica symmetry breaking in the 'small world' spin glass*, J. Stat. Mech. P11007 (2005).

[34] M. Mézard and G. Parisi, *The Bethe lattice spin glass revisited*, Eur. Phys. J. B **20**, 217 (2001).

[35] L. Viana and A. J. Bray, *Phase diagrams for dilute spin glasses*, J. Phys. C **18**, 3037 (1985).

[36] R. Monasson, *Optimization problems and replica symmetry breaking in finite connectivity spin glasses*, J. Phys. A **31**, 513 (1998).

[37] J. R. L. de Almeida and D. J. Thouless, *Stability of the Sherrington-Kirkpatrick solution of a spin glass model*, J. Phys. A **11**, 983 (1978).

[38] P. Cizeau and J. P. Bouchaud, *Mean field theory of dilute spin-glasses with power-law interactions*, J. Phys. A **26**, L187 (1993).

[39] I. Neri, F. L. Metz, and D. Bollé, *The phase diagram of Lévy spin glasses*, J. Stat. Mech. P01010 (2010).

[40] K. Janzen, A. Engel, and M. Mézard, *Thermodynamics of the Lévy spin glass*, Phys. Rev. E **82**, 021127 (2010).

[41] K. Binder, *Critical properties from Monte Carlo coarse graining and renormalization*, Phys. Rev. Lett. **47**, 693 (1981).

[42] D. Larson, H. G. Katzgraber, M. A. Moore, and A. P. Young, *Numerical studies of a one-dimensional 3-spin spin-glass model with long-range interactions*, Phys. Rev. B **81**, 064415 (2010).

[43] F. Cooper, B. Freedman, and D. Preston, *Solving $\phi^4_{1,2}$ theory with Monte Carlo*, Nucl. Phys. B **210**, 210 (1982).

[44] M. Palassini and S. Caracciolo, *Universal Finite-Size Scaling Functions in the 3D Ising Spin Glass*, Phys. Rev. Lett. **82**, 5128 (1999).

[45] H. G. Ballesteros, A. Cruz, L. A. Fernandez, V. Martin-Mayor, J. Pech, J. J. Ruiz-Lorenzo, A. Tarancon, P. Tellez, C. L. Ullod, and C. Ungil, *Critical behavior of the three-dimensional Ising spin glass*, Phys. Rev. B **62**, 14237 (2000).

[46] V. Martín-Mayor, A. Pelissetto, and E. Vicari, *Critical structure factor in Ising systems*, Phys. Rev. E **66**, 026112 (2002).

[47] K. Hukushima and K. Nemoto, *Exchange Monte Carlo method and application to spin glass simulations*, J. Phys. Soc. Jpn. **65**, 1604 (1996).

[48] H. G. Katzgraber, M. Palassini, and A. P. Young, *Monte Carlo simulations of spin glasses at low temperatures*, Phys. Rev. B **63**, 184422 (2001).

[49] H. G. Katzgraber, D. Larson, and A. P. Young, *Study of the de Almeida-Thouless line using power-law diluted one-dimensional Ising spin glasses*, Phys. Rev. Lett. **102**, 177205 (2009).

[50] S. N. Dorogovtsev, A. V. Goltsev, and J. F. F. Mendes, *Critical phenomena in complex networks*, Rev. Mod. Phys. **80**, 1275 (2008).

[51] Note that all our numerical estimates for the critical temperatures are approximately 5% above the analytically-determined values. Further studies would be needed to better understand this small deviation. The small systematic deviation could be, for example, attributed to corrections to scaling or the fact that the analytical results take all graphs to be equally weighted, whereas this is not the case in the numerical results. However, we emphasize that the agreement is remarkably good.

[52] H. G. Katzgraber, M. Körner, and A. P. Young, *Universality in three-dimensional Ising spin glasses: A Monte Carlo study*, Phys. Rev. B **73**, 224432 (2006).

[53] M. Wittmann and A. P. Young, *Spin glasses in the nonextensive regime*, Phys. Rev. E **85**, 041104 (2012).